©Civil-Comp Press, 2012
Proceedings of the Eleventh International Conference
on Computational Structures Technology,
B.H.V. Topping, (Editor),
Civil-Comp Press, Stirlingshire, Scotland

Paper 158

Rheological-Dynamical Limit Analysis of Reinforced Concrete Folded Plate Structures using the Harmonic Coupled Finite-Strip Method

D.D. Milašinović[1], D. Goleš[1], A. Borković[2], D. Kukaras[1]
A. Landović[1], Ž. Živanov[3] and P. Rakić[3]
[1] Faculty of Civil Engineering, University of Novi Sad, Subotica, Serbia
[2] Faculty of Architecture and Civil Engineering
University of Banjaluka, Bosnia and Herzegovina
[3] Faculty of Technical Sciences, University of Novi Sad, Serbia

Abstract

Currently the finite-element method (FEM) is considered as the most promising analysis tool among the existing methods of analysis which are usually based on the continuum mechanics approach, but accuracy of the FEM solutions for nonlinear problems of solid mechanics can be hardly guaranteed and the computing cost is still prohibitive. To overcome such a drawback of the nonlinear FEM including their application to reinforced concrete folded plate structures, this paper presents the application of the harmonic coupled finite-strip method (HCFSM) to structure stability analysis. The theoretical stress-strain relations of various concrete strength classes and reinforcement, knowing only the minimum number of mechanical material parameters that come from standard test procedures, are determined from the rheological-dynamical analogy (RDA). As an illustrative example, a feasible reinforced concrete folded plate structure is analysed in detail. The ultimate resistance of two characteristic cross sections of a folded plate structure is calculated using working diagrams of concrete and steel according to Eurocode 2 and according to the RDA. Diagrams of interaction N_u-M_u are drawn for several combinations of material working diagrams and are mutually compared.

Keywords: harmonic coupled finite-strip method, rheological-dynamical limit analysis.

1 Introduction

The problem of the stability analysis of reinforced concrete folded plate structures has gained importance during the past years due to the application of various reinforced concrete materials and their utilization of high working stress. In the past years, the present problem was treated in the scope of many research projects theoretically and experimentally. Most of these projects are, however, subject to

several restrictions, especially with regard to cross-sectional geometry, real mechanical properties of materials, and nonlinear finite element solutions which can be hardly guaranteed.

The conventional finite strip method (FSM) is based on the harmonic functions, and proved to be efficient tool for analyzing a great deal of structures for which both geometry and material properties can be considered as constants along a main direction, straight or curved, while only the loading distribution may vary. This method was pioneered by Cheung [1].

In this work we present the semi-analytical harmonic coupled finite strip method (HCFSM) for geometric non-linear analysis of reinforced concrete plate structures under multiple loading conditions. This method takes into account the important influence of the interaction between the buckling modes [2]. In contrast, the FSM, in its usual form, ignores this interaction and therefore cannot be used in the structure stability analysis. The risk of structural instability is analysed as realistically as possible under the influence of realistic composite material behaviour.

The aim of this paper is based on the rheological-dynamical limit analysis to predict the ultimate resistance of structure. On the basis of the RDA, the working diagrams of concrete and steel are built, representing simultaneous stress-strain pairs. The RDA working diagrams are then compared with recommended diagrams from the Eurocode 2 (EC 2).

As an illustrative example, a feasible reinforced concrete folded plate structure is analyzed in detail. Effects of applied actions are firstly calculated using linear FSM. Limit state design (ultimate and serviceability) of characteristic cross sections is then performed according to the currently valid Serbian technical regulations for concrete and reinforced concrete, using the partial factor method. The ultimate resistance of so designed two characteristic cross sections is determined from diagrams of interaction (N_u-M_u). They are drawn according to Eurocode 2 and RDA working diagrams. The ultimate resistance (N_u) of cross sections is then compared with effects of applied actions (N) calculated by FSM and HCFSM. The global safety factors γ, defined as the ratio between N_u and normal force due to service loading with the same excentricity $e=M/N$ (M is the bending moment of cross-section due to service load), are also compared at the end.

2 Harmonic-coupled Finite-Strip Method and Stability Analysis

2.1 Harmonic-coupled Finite-Strip Method

Typical flat plate structures under consideration here are simply supported by diaphragms and may have arbitrary longitudinal edge conditions. For these structures, the design process should lead to define the optimal morphology of the transversal cross-section, which means its geometry, size, shape and topology.

In the FSM, which combines elements of the classical Ritz and the finite-element methods, the general form of the displacement function can be written as a product of polynomials and trigonometric functions

$$f = \sum_{m=1}^{r} Y_m(y) \sum_{k=1}^{c} \mathbf{N}_k(x) \mathbf{q}_{km} \tag{1}$$

where $Y_m(y)$ are functions from the Ritz method and $\boldsymbol{N}_k(x)$ are interpolation functions from the finite-element method. We define the local Degrees Of Freedom (DOFs) as the displacements and rotation of a nodal line (DOFs=4). The DOFs are also called generalized coordinates.

The nonlinear strain-displacement relations in the finite strip can be predicted by the combination of the plane elasticity and the Kirchhoff plate theory. Using this assumption in the Green-Lagrange strain tensor (2) for in-plane nonlinear strains gives Green-Lagrange HCFSM formulation. Also that, neglecting lower-order terms in a manner consistent with the usual von Karman assumptions gives HCFSM von Karman formulation.

$$\varepsilon_{ij} = 1/2\left(u_{i,j} + u_{j,i} + u_{k,i}u_{k,j}\right) \tag{2}$$

The essential feature of geometric nonlinearity is that equilibrium equations must be written with respect to the deformed geometry – which is not known in advance. As a preliminary to tracing the equilibrium paths, it is necessary to determine the total potential energy of the structure as a function of the global DOFs. The steps in the computation are detailed discussed in [2].

The total potential energy of a strip is designated Π and is expressed with respect to the local DOFs by the HCFSM.

$$\begin{aligned}
\Pi = U + W = \left(U_m + U_b\right) + W = &\left(1/2\int_A \mathbf{q}_u^T \mathbf{B}_{u1}^T \mathbf{D}_{11} \mathbf{B}_{u1} \mathbf{q}_u dA + 1/2\int_A \mathbf{q}_w^T \mathbf{B}_{w3}^T \mathbf{D}_{22} \mathbf{B}_{w3} \mathbf{q}_w dA\right) + \\
&+\left[\begin{array}{l} 1/8\int_A \mathbf{q}_w^T \mathbf{B}_{w2}^T \mathbf{W}^T \mathbf{B}_{w1}^T \mathbf{D}_{11} \mathbf{B}_{w1} \mathbf{W} \mathbf{B}_{w2} \mathbf{q}_w dA + 1/4\int_A \mathbf{q}_w^T \mathbf{B}_{w2}^T \mathbf{W}^T \mathbf{B}_{w1}^T \mathbf{D}_{11} \mathbf{B}_{u1} \mathbf{q}_u dA + \\ +1/4\int_A \mathbf{q}_u^T \mathbf{B}_{u1}^T \mathbf{D}_{11} \mathbf{B}_{w1} \mathbf{W} \mathbf{B}_{w2} \mathbf{q}_w dA \end{array}\right] + \\
&+\left\{\begin{array}{l} 1/8\int_A \mathbf{q}_u^{uT} \mathbf{B}_{u2}^{uT} \mathbf{U}^T \mathbf{B}_{u1}^{uT} \mathbf{D}_{11} \mathbf{B}_{u1}^u \mathbf{U} \mathbf{B}_{u2}^u \mathbf{q}_u^u dA + 1/4\int_A \mathbf{q}_u^{uT} \mathbf{B}_{u4}^{uT} \mathbf{D}_{11} \mathbf{B}_{u1}^u \mathbf{U} \mathbf{B}_{u2}^u \mathbf{q}_u^u dA + \\ +1/4\int_A \mathbf{q}_u^{uT} \mathbf{B}_{u2}^{uT} \mathbf{U}^T \mathbf{B}_{u1}^{uT} \mathbf{D}_{11} \mathbf{B}_{u4}^u \mathbf{q}_u^u dA + \\ +1/4\int_A \mathbf{q}_u^{vT} \mathbf{B}_{u5}^{vT} \mathbf{D}_{11} \mathbf{B}_{u1}^u \mathbf{U} \mathbf{B}_{u2}^u \mathbf{q}_u^u dA + 1/4\int_A \mathbf{q}_u^{uT} \mathbf{B}_{u2}^{uT} \mathbf{U}^T \mathbf{B}_{u1}^{uT} \mathbf{D}_{11} \mathbf{B}_{u5}^v \mathbf{q}_u^v dA + \\ +1/8\int_A \mathbf{q}_w^T \mathbf{B}_{w2}^T \mathbf{W}^T \mathbf{B}_{w1}^T \mathbf{D}_{11} \mathbf{B}_{u1}^u \mathbf{U} \mathbf{B}_{u2}^u \mathbf{q}_u^u dA + 1/8\int_A \mathbf{q}_u^{uT} \mathbf{B}_{u2}^{uT} \mathbf{U}^T \mathbf{B}_{u1}^{uT} \mathbf{D}_{11} \mathbf{B}_{w1} \mathbf{W} \mathbf{B}_{w2} \mathbf{q}_w dA \end{array}\right\} - \\
&-\int_A \mathbf{q}^T \mathbf{A}^T \mathbf{p} dA
\end{aligned} \tag{3}$$

The multiplication results of the membrane and bending actions in the first bracket of Eq. (3) are uniquely defined and uncoupled, whilst those in second [von Karman assumptions] and third bracket {Green-Lagrange approach} are functions of the displacements u_0, v_0 and w. Consequently, the membrane and bending actions are coupled in many ways.

The conventional and the geometric stiffness matrices are, respectively:

$$(\hat{\mathbf{K}}_{uu} = \int_A \mathbf{B}_{u1}^T \mathbf{D}_{11} \mathbf{B}_{u1} dA\,,\ \hat{\mathbf{K}}_{ww} = \int_A \mathbf{B}_{w3}^T \mathbf{D}_{22} \mathbf{B}_{w3} dA\,) \tag{4}$$

$$[\,\tilde{\mathbf{K}}_{ww} = \int_A \mathbf{B}_{w2}^T \mathbf{W}^T \mathbf{G}_1 \mathbf{W} \mathbf{B}_{w2} dA\,,\ \tilde{\mathbf{K}}_{wu} = \int_A \mathbf{B}_{w2}^T \mathbf{W}^T \mathbf{G}_2 dA\,,\ \tilde{\mathbf{K}}_{uw} = \int_A \mathbf{G}_2^T \mathbf{W} \mathbf{B}_{w2} dA\,] \tag{5}$$

$$\{\,\tilde{\mathbf{K}}_{uu}^{uu} = \int_A \mathbf{B}_{u2}^{uT} \mathbf{U}^T \mathbf{G}_3 \mathbf{U} \mathbf{B}_{u2}^u dA\,,\ \tilde{\mathbf{K}}_{uu}^{uu*} = \int_A \mathbf{G}_4 \mathbf{U} \mathbf{B}_{u2}^u dA\,,\ \tilde{\mathbf{K}}_{uu}^{uu**} = \int_A \mathbf{B}_{u2}^{uT} \mathbf{U}^T \mathbf{G}_4^T dA\,,\ \tilde{\mathbf{K}}_{uu}^{vu} = \int_A \mathbf{G}_5 \mathbf{U} \mathbf{B}_{u2}^u dA\,,$$
$$\tilde{\mathbf{K}}_{uu}^{uv} = \int_A \mathbf{B}_{u2}^{uT} \mathbf{U}^T \mathbf{G}_5^T dA\,,\ \tilde{\mathbf{K}}_{wu}^{u} = \int_A \mathbf{B}_{w2}^T \mathbf{W}^T \mathbf{G}_6 \mathbf{U} \mathbf{B}_{u2}^u dA\,,\ \tilde{\mathbf{K}}_{uw}^{u} = \int_A \mathbf{B}_{u2}^{uT} \mathbf{U}^T \mathbf{G}_6^T \mathbf{W} \mathbf{B}_{w2} dA\,\},$$

where

$$[\,\mathbf{G}_1 = \mathbf{B}_{w1}^T \mathbf{D}_{11} \mathbf{B}_{w1}\,,\ \mathbf{G}_2 = \mathbf{B}_{w1}^T \mathbf{D}_{11} \mathbf{B}_{u1}\,], \tag{6}$$
$$\{\,\mathbf{G}_3 = \mathbf{B}_{u1}^{uT} \mathbf{D}_{11} \mathbf{B}_{u1}^u\,,\ \mathbf{G}_4 = \mathbf{B}_{u4}^{uT} \mathbf{D}_{11} \mathbf{B}_{u1}^u\,,\ \mathbf{G}_5 = \mathbf{B}_{u5}^{vT} \mathbf{D}_{11} \mathbf{B}_{u1}^u\,,\ \mathbf{G}_6 = \mathbf{B}_{w1}^T \mathbf{D}_{11} \mathbf{B}_{u1}^u\,\}.$$

The geometric stiffness matrix of structure is built by summing overlapping terms of the component strip matrices; in the same way that conventional stiffness matrix of structure is built by summing terms of the conventional strip matrices using the transformation matrices between the local and global displacements [2].

2.2 Stability Analysis

Since the principle of the stationary potential energy states that the necessary condition of the equilibrium of any given state is that the variation of the total potential energy of the considered structure is equal to zero, we have the following relation:

$$\delta\Pi = 0 \tag{7}$$

Eq. (7) is satisfied for an arbitrary value of the variations of parameters $\delta\mathbf{q}_m^T$. Thus we have the following conditions, which must be satisfied for any harmonic *m*:

$$\frac{\partial\Pi}{\partial\mathbf{q}_m^T} = \mathbf{0} \tag{8}$$

Next, we calculate derivatives of the total potential energy of a strip and finally, we get a non-homogeneous and nonlinear set of algebraic equations (9), which are the searched stability equations.

$$\left(\hat{\mathbf{K}}_{uu}\mathbf{q}_u + \hat{\mathbf{K}}_{ww}\mathbf{q}_w\right) + \left[1/2\,\tilde{\mathbf{K}}_{ww}\mathbf{q}_w + 1/2\,\tilde{\mathbf{K}}_{wu}\mathbf{q}_u + 1/4\,\tilde{\mathbf{K}}_{uw}\mathbf{q}_w\right] +$$
$$+\begin{Bmatrix} 1/2\,\tilde{\mathbf{K}}_{uu}^{uu}\mathbf{q}_u^u + 3/4\,\tilde{\mathbf{K}}_{uu}^{uu*}\mathbf{q}_u^u + 3/4\,\tilde{\mathbf{K}}_{uu}^{uu**}\mathbf{q}_u^u + 1/4\,\tilde{\mathbf{K}}_{uu}^{vu}\mathbf{q}_u^u + \\ +1/2\,\tilde{\mathbf{K}}_{uu}^{uv}\mathbf{q}_u^v + 1/4\,\tilde{\mathbf{K}}_{wu}^{u}\mathbf{q}_u^u + 1/4\,\tilde{\mathbf{K}}_{uw}^{u}\mathbf{q}_w \end{Bmatrix} - \mathbf{Q} = \mathbf{0} \tag{9}$$

We can visualize the construction of a strip stiffness matrix, which is composed of twelve block matrices. Assembling block matrices into conventional/geometric stiffness matrix of each strip is performed according to the scheme presented in Fig. 1, where: ST1=$\hat{\mathbf{K}}_{uu}$, ST2=$\hat{\mathbf{K}}_{ww}$, ST3=$\tilde{\mathbf{K}}_{ww}$, ST4=$\tilde{\mathbf{K}}_{wu}$, ST5=$\tilde{\mathbf{K}}_{uw}$, ST6=$\tilde{\mathbf{K}}_{uu}^{uu}$, ST7=$\tilde{\mathbf{K}}_{uu}^{uu*}$, ST8=$\tilde{\mathbf{K}}_{uu}^{uu**}$, ST9=$\tilde{\mathbf{K}}_{uu}^{vu}$, ST10=$\tilde{\mathbf{K}}_{uu}^{uv}$, ST11=$\tilde{\mathbf{K}}_{wu}^{u}$ and ST12=$\tilde{\mathbf{K}}_{uw}^{u}$ (ST5=ST4^T, ST8=ST7^T, ST10=ST9^T, ST12=ST11^T).

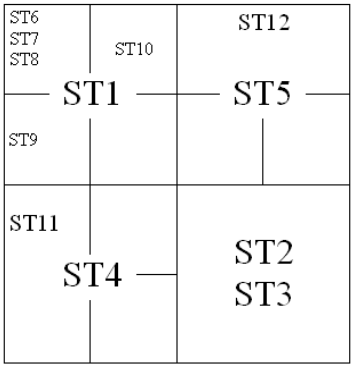

Figure 1: Strip stiffness matrix assembling

For equilibrium, the principle of stationary potential energy requires that:

$$\mathbf{R} = \partial\Pi / \partial \mathbf{q}^T = \left[\hat{\mathbf{K}} + \tilde{\mathbf{K}}\right]\mathbf{q} - \mathbf{Q} = \mathbf{K}\mathbf{q} - \mathbf{Q} = \mathbf{0} \tag{10}$$

where Π is a function of the displacements $\boldsymbol{q}$, and $\boldsymbol{R}$ represent the gradient or residual force vector, which is generally nonzero for some approximate displacement vector $\boldsymbol{q_0}$ (the subscript 0 denotes an old value). It is assumed that a better approximation is given by:

$$\mathbf{q}_n = \mathbf{q}_0 + \boldsymbol{\delta}_0 . \tag{11}$$

where subscript n denotes a new value.
Taylor's expansion of Eq. (10) yields:

$$\mathbf{R}_n = \mathbf{R}(\mathbf{q}_0 + \boldsymbol{\delta}_0) = \mathbf{R}(\mathbf{q}_0) + \bar{\mathbf{K}}_0\boldsymbol{\delta}_0 + \ldots = \mathbf{R}_0 + \bar{\mathbf{K}}_0\boldsymbol{\delta}_0 + \ldots \tag{12}$$

where $\bar{\mathbf{K}}_0 = \partial\mathbf{R}/\partial\mathbf{q}$ is the matrix of second partial derivatives of Π calculated at $\boldsymbol{q_0}$ (i.e. the tangent stiffness matrix or Hessian matrix). Setting Eq. (12) to zero and considering only linear terms in $\boldsymbol{\delta_0}$ gives the standard expression for Newton-Raphson iteration:

$$\boldsymbol{\delta}_0 = -\bar{\mathbf{K}}_0^{-1}\mathbf{R}_0 . \tag{13}$$

Using this approach, a further iteration yields:

$$\boldsymbol{\delta}_n = \bar{\mathbf{K}}_n^{-1}\mathbf{R}_n \tag{14}$$

where $\bar{\mathbf{K}}_n = \partial\mathbf{R}/\partial\mathbf{q}$ at $\boldsymbol{q}_n$.

In addition, the blocks of the conventional and geometric tangent stiffness matrix of each strip are:

$$\hat{\bar{\mathbf{K}}} = \begin{bmatrix} \hat{\mathbf{K}}_{uu} & \mathbf{0} \\ \mathbf{0} & \hat{\mathbf{K}}_{ww} \end{bmatrix}. \tag{15}$$

$$\begin{aligned} \tilde{\bar{\mathbf{K}}} = & \begin{bmatrix} \mathbf{0} & 1/2\,\tilde{\mathbf{K}}_{uw} \\ 1/2\,\tilde{\mathbf{K}}_{wu} & 3/2\,\tilde{\mathbf{K}}_{ww} \end{bmatrix} + \\ & + \begin{bmatrix} 3/2\,\tilde{\mathbf{K}}_{uu}^{uu} + 3/2\,\tilde{\mathbf{K}}_{uu}^{uu*} + 3/2\,\tilde{\mathbf{K}}_{uu}^{uu**} & 1/2\,\tilde{\mathbf{K}}_{uu}^{uv} \\ 1/2\,\tilde{\mathbf{K}}_{uu}^{vu} & \mathbf{0} \end{bmatrix} + \begin{bmatrix} \mathbf{0} & 1/2\,\tilde{\mathbf{K}}_{uw}^{u} \\ 1/2\,\tilde{\mathbf{K}}_{wu}^{u} & \mathbf{0} \end{bmatrix} \end{aligned} \tag{16}$$

Comparing these expressions with Eq. (9), it is apparent that the conventional stiffness matrix remains unchanged, while the geometric tangent matrix becomes symmetrical.

The loss of stability of static equilibrium states of structures subjected to conservative loads is in general known as static buckling of the structure. For conservative systems, the principle of minimum of the total potential energy can be used to test the stability of a structure (static equilibriums are extremes of the total potential energy). The Hessian with respect to the local DOFs is denoted as the tangent stiffness matrix, of each strip i.e.:

$$\bar{\mathbf{K}} = \left[\hat{\bar{\mathbf{K}}} + \tilde{\bar{\mathbf{K}}} \right] \tag{17}$$

The (local) stability of equilibrium states of conservative systems by HCFSM can be assessed by looking at the eigenvalues of the tangent stiffness matrix of structure (TSMS) $\bar{\mathbf{K}}_{(DOFs \cdot r \cdot (n+1)) \cdot (DOFs \cdot r \cdot (n+1))}$ with (n+1) nodal lines, which are all real, since tangent stiffness matrix of the strip is a symmetric matrix.

A typical rectangular plate is divided into (n) finite strips with (n+1) nodal lines. Let λ_i denote the ith eigenvalue of

$$\bar{\mathbf{K}}_{(DOFs \cdot r \cdot (n+1)) \cdot (DOFs \cdot r \cdot (n+1))} \tag{18}$$

Based on theorems of Lagrange-Dirichlet and Lyapunov [3] it can be concluded that an equilibrium state is stable if all λ_i>0, while an equilibrium state is unstable if one or more λ_i<0. If along a load-path (IINCS=1, NINCS), at some equilibrium state one or more λ_i=0, this equilibrium state is denoted as a critical state. Static buckling refers in general to case where, starting from some stable state, a critical state is reached along the load-path. Buckling occurs where the matrix becomes singular.

The integral expressions contain the products of trigonometric functions with higher-order exponents, and therefore the orthogonality characteristics are no longer valid. To calculate the blocks of the tangent geometric stiffness matrix, it would be necessary to know values for the basic unknowns in all series terms at the moment of their computation. Therefore, the only possible way to form the tangent stiffness matrix using the HCFSM is to take into account all series terms.

Depending on the particular problem under consideration, the Green-Lagrange nonlinear contributions, Eq. (2) in a manner consistent the von Karman assumptions may be safely ignored. Otherwise the next seven blocks must be added

$$\tilde{\mathbf{K}}^{uu}_{uumn} = \int_A \sum_{v,p=1}^{r} \sum_{s,t=1}^{r} \mathbf{B}^{uT}_{u2m} \mathbf{U}^T_s \mathbf{B}^{uT}_{u1t} \mathbf{D}_{11} \mathbf{B}^{u}_{u1v} \mathbf{U}_p \mathbf{B}^{u}_{u2n} dA \,,$$

$$\tilde{\mathbf{K}}^{uu*}_{uumn} = \int_A \sum_{s,p=1}^{r} \mathbf{B}^{uT}_{u4m} \mathbf{D}_{11} \mathbf{B}^{u}_{u1s} \mathbf{U}_p \mathbf{B}^{u}_{u2n} dA \,,$$

$$\tilde{\mathbf{K}}^{uu**}_{uumn} = \int_A \sum_{s,p=1}^{r} \mathbf{B}^{uT}_{u2m} \mathbf{U}^T_s \mathbf{B}^{uT}_{u1p} \mathbf{D}_{11} \mathbf{B}^{u}_{u4n} dA \,,$$

$$\tilde{\mathbf{K}}^{vu}_{uumn} = \int_A \sum_{s,p=1}^{r} \mathbf{B}^{vT}_{u5m} \mathbf{D}_{11} \mathbf{B}^{u}_{u1s} \mathbf{U}_p \mathbf{B}^{u}_{u2n} dA \,,$$

$$\tilde{\mathbf{K}}^{uv}_{uumn} = \int_A \sum_{s,p=1}^{r} \mathbf{B}^{uT}_{u2m} \mathbf{U}^T_s \mathbf{B}^{uT}_{u1p} \mathbf{D}_{11} \mathbf{B}^{v}_{u5n} dA \,,$$

$$\tilde{\mathbf{K}}^{u}_{wumn} = \int_A \sum_{v,p=1}^{r} \sum_{s,t=1}^{r} \mathbf{B}^{T}_{w2m} \mathbf{W}^{T}_{s} \mathbf{B}^{T}_{w1t} \mathbf{D}_{11} \mathbf{B}^{u}_{u1v} \mathbf{U}_{p} \mathbf{B}^{u}_{u2n} dA \,,$$

$$\tilde{\mathbf{K}}^{u}_{uwmn} = \int_A \sum_{v,p=1}^{r} \sum_{s,t=1}^{r} \mathbf{B}^{uT}_{u2m} \mathbf{U}^{T}_{s} \mathbf{B}^{uT}_{u1t} \mathbf{D}_{11} \mathbf{B}_{w1v} \mathbf{W}_{p} \mathbf{B}_{w2n} dA \,. \tag{19}$$

The forces ($N_x=t\sigma_x$, $N_y=t\sigma_y$, $N_{xy}=t\tau_{xy}$) and moments (M_x, M_y, M_{xy}) are related to the strains through the material properties of the strip. In the present formulation the more general case of orthotropic properties is assumed.

$$\hat{\mathbf{N}}_{um} = t \begin{bmatrix} \mathbf{N}^{u}_{u,x} Y^{u}_{um}\, E_x \big/ \left(1-\mu_x\mu_y\right) \mathbf{q}^{u}_{um} + \mathbf{N}^{v}_{u} Y^{v}_{u,ym}\, \mu_x E_y \big/ \left(1-\mu_x\mu_y\right) \mathbf{q}^{v}_{um} \\ \mathbf{N}^{u}_{u,x} Y^{u}_{um}\, \mu_x E_y \big/ \left(1-\mu_x\mu_y\right) \mathbf{q}^{u}_{um} + \mathbf{N}^{v}_{u} Y^{v}_{u,ym}\, E_y \big/ \left(1-\mu_x\mu_y\right) \mathbf{q}^{v}_{um} \\ \mathbf{N}^{u}_{u} Y^{u}_{u,ym} G \mathbf{q}^{u}_{um} + \mathbf{N}^{v}_{u,x} Y^{v}_{um} G \mathbf{q}^{v}_{um} \end{bmatrix},$$

$$\tilde{\mathbf{N}}_{wm} = t \begin{bmatrix} \mathbf{N}_{w,x} Y_{wm}\, E_x \big/ \left(1-\mu_x\mu_y\right) \mathbf{q}_{wm} \mathbf{N}_{w,x} Y_{wm} \mathbf{q}_{wm} + \mathbf{N}_{w} Y_{w,ym}\, \mu_x E_y \big/ \left(1-\mu_x\mu_y\right) \mathbf{q}_{wm} \mathbf{N}_{w} Y_{w,ym} \mathbf{q}_{wm} \\ \mathbf{N}_{w,x} Y_{wm}\, \mu_x E_y \big/ \left(1-\mu_x\mu_y\right) \mathbf{q}_{wm} \mathbf{N}_{w,x} Y_{wm} \mathbf{q}_{wm} + \mathbf{N}_{w} Y_{w,ym}\, E_y \big/ \left(1-\mu_x\mu_y\right) \mathbf{q}_{wm} \mathbf{N}_{w} Y_{w,ym} \mathbf{q}_{wm} \\ \mathbf{N}_{w} Y_{w,ym} G \mathbf{q}_{wm} \mathbf{N}_{w,x} Y_{wm} \mathbf{q}_{wm} + \mathbf{N}_{w,x} Y_{wm} G \mathbf{q}_{wm} \mathbf{N}_{w} Y_{w,ym} \mathbf{q}_{wm} \end{bmatrix},$$

$$\tilde{\mathbf{N}}^{u}_{um} = t \begin{bmatrix} \mathbf{N}^{u}_{u,x} Y^{u}_{um}\, E_x \big/ \left(1-\mu_x\mu_y\right) \mathbf{q}^{u}_{um} \mathbf{N}^{u}_{u,x} Y^{u}_{um} \mathbf{q}^{u}_{um} + \mathbf{N}^{u}_{u} Y^{u}_{u,ym}\, \mu_x E_y \big/ \left(1-\mu_x\mu_y\right) \mathbf{q}^{u}_{um} \mathbf{N}^{u}_{u} Y^{u}_{u,ym} \mathbf{q}^{u}_{um} \\ \mathbf{N}^{u}_{u,x} Y^{u}_{um}\, \mu_x E_y \big/ \left(1-\mu_x\mu_y\right) \mathbf{q}^{u}_{um} \mathbf{N}^{u}_{u,x} Y^{u}_{um} \mathbf{q}^{u}_{um} + \mathbf{N}^{u}_{u} Y^{u}_{u,ym}\, E_y \big/ \left(1-\mu_x\mu_y\right) \mathbf{q}^{u}_{um} \mathbf{N}^{u}_{u} Y^{u}_{u,ym} \mathbf{q}^{u}_{um} \\ \mathbf{N}^{u}_{u} Y^{u}_{u,ym} G \mathbf{q}^{u}_{um} \mathbf{N}^{u}_{u,x} Y^{u}_{um} \mathbf{q}^{u}_{um} + \mathbf{N}^{u}_{u,x} Y^{u}_{um} G \mathbf{q}^{u}_{um} \mathbf{N}^{u}_{u} Y^{u}_{u,ym} \mathbf{q}^{u}_{um} \end{bmatrix},$$

$$\hat{\mathbf{M}}_{wm} = \left(t^3/12\right) \begin{bmatrix} -\mathbf{N}_{w,xx} Y_{wm}\, E_x \big/ \left(1-\mu_x\mu_y\right) \mathbf{q}_{wm} - \mathbf{N}_{w} Y_{w,yym}\, \mu_x E_y \big/ \left(1-\mu_x\mu_y\right) \mathbf{q}_{wm} \\ -\mathbf{N}_{w,xx} Y_{wm}\, \mu_x E_y \big/ \left(1-\mu_x\mu_y\right) \mathbf{q}_{wm} - \mathbf{N}_{w} Y_{w,yym}\, E_y \big/ \left(1-\mu_x\mu_y\right) \mathbf{q}_{wm} \\ -2\mathbf{N}_{w,x} Y_{w,ym} G \mathbf{q}_{wm} \end{bmatrix}. \tag{20}$$

3 Rheological-Dynamical and EC 2 Limit Analysis

3.1 Rheological-Dynamical Analogy Short Overview

In the material fatigue investigations, both stress $\sigma(t)$ and total (inelastic) strain $\varepsilon(t)=\varepsilon_{el}+\varepsilon_{ve}(t)+\varepsilon_{vp}(t)$ are functions of time. During the production process, material yielding takes place. Various design techniques have been developed, and rheology, as a science, gives us an opportunity of assembling and processing differential equations with respect to the rheological models. Graphically demonstrated, the stress-strain pairs resulting from the same instants of time give us isochronous stress-strain diagrams.

If the total strain is represented by the sum of the elastic, viscoelastic (VE) and viscoplastic (VP) components, each isochronous stress-strain diagram of a long prismatic rod (e.g., with a square or circular initial cross-section A_0), which is shown in Fig. 2a, can accurately be approximated by the rheological body consisting of five elements. The model of the rheological body is shown in Fig. 2b, using the following symbols: N for the Newtonian dashpot, StV for Saint-Venant's body, H for the Hookean spring, | for parallel connection and — for connection in series.

Since the Hokean spring, Kelvin's body ($K=H|N$) and VP body (StV$|N$) are connected in series, the stresses $\sigma(t)$ in all bodies are equal.

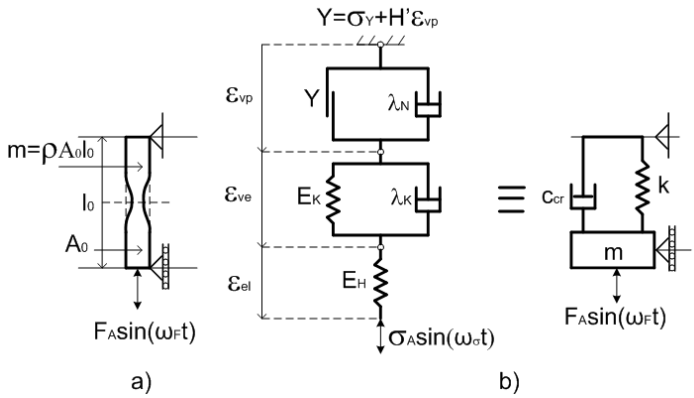

Figure 2: Rheological-dynamical analogy of a prismatic column with reduced cross-section

The governing differential equation has been derived in Ref. [4]

$$\ddot{\varepsilon}(t)+\dot{\varepsilon}(t)\left(\frac{E_K}{\lambda_K}+\frac{H'}{\lambda_N}\right)+\varepsilon(t)\frac{E_K H'}{\lambda_K\lambda_N}=\frac{\ddot{\sigma}(t)}{E_H}+\dot{\sigma}(t)\left(\frac{E_K}{\lambda_K E_H}+\frac{H'}{\lambda_N E_H}+\frac{1}{\lambda_K}+\frac{1}{\lambda_N}\right)+$$
$$+\sigma(t)\left(\frac{E_K}{\lambda_K\lambda_N}+\frac{H'}{\lambda_K\lambda_N}+\frac{E_K H'}{\lambda_K\lambda_N E_H}\right)-\sigma_Y\frac{E_K}{\lambda_K\lambda_N} \tag{21}$$

where σ_Y is the yield stress. The yield condition is $Y=\sigma_Y+H'\varepsilon_{vp}(t)$. Four constants at fixed step time are as follows: VE normal viscosity λ_K, VP normal viscosity λ_N, VE modulus E_K and VP modulus H'. However, these constants cannot easily be determined by the physical experiments, especially Trouton's normal viscosities λ_K and λ_N. The corresponding homogeneous equation is as follows:

$$\ddot{\varepsilon}(t)\lambda_K\lambda_N+\dot{\varepsilon}(t)\left(E_K\lambda_N+H'\lambda_K\right)+\varepsilon(t)E_K H'=0 \tag{22}$$

On the other hand, a mechanical longitudinal disturbance (strain) propagates in an elastic medium at the finite initial phase velocity $v_0=\sqrt{E_H/\rho}$. The vibration at an arbitrary point M of the rod lags in the phase behind that at the source of the wave. If l_0 is the initial distance between two ends of the rod (standing wave length), the time difference is $t-t_0=T_K^D=l_0/v_0$. The parameter T_K^D represents a dynamic time of retardation. The natural angular frequency of the discrete dynamical model, which represents an undamped free longitudinal vibration of the rod, is as follows:

$$\omega=\sqrt{\frac{k}{m}}=\sqrt{\frac{E_H A_0}{l_0}\frac{1}{\rho A_0 l_0}}=\frac{v_0}{l_0}=\frac{1}{T_K^D}\Rightarrow T_K^D=\frac{l_0}{v_0}=\frac{1}{\omega} \tag{23}$$

Bearing in mind Eq. (22), an expression similar to Eq. (23) can be formulated setting the rheological model of the rod into the state of critical viscous damping ($c=c_{cr}$), where $E_K/\lambda_K=H'/\lambda_N$, $\lambda_K=E_K T_K$, $\lambda_N=H'T^*$, $T_K=T^*=T_K^D$:

$$\omega=\sqrt{\frac{E_K H'}{\lambda_K\lambda_N}}=\sqrt{\frac{1}{T_K T^*}}=\frac{1}{T_K^D} \tag{24}$$

According to formulas (23) and (24) we shall have

$$\sqrt{\frac{E_H}{\rho}}\frac{1}{l_0}=\sqrt{\frac{E_K H'}{\lambda_K \lambda_N}} \Rightarrow \lambda_K \lambda_N = \frac{E_K H' \gamma l_0^2}{E_H g} \Rightarrow \frac{\lambda_K \lambda_N}{\gamma} = \frac{E_K H' A_0 l_0^2 \rho}{E_H \gamma A_0}$$
$$\Rightarrow m = \frac{\lambda_K \lambda_N}{\gamma} = k\left(T_K^D\right)^2,\ k = \frac{E_K H'}{\gamma},\ c_{cr} = 2\sqrt{km} = 2kT_K^D \tag{25}$$

Consequently, propagation of longitudinal elastic waves represents a physical basis for the analogy between two different physical phenomena. The RDA Eq. (22) becomes:

$$\ddot{\varepsilon}(t)m + \dot{\varepsilon}(t)c_{cr} + \varepsilon(t)k = 0 \tag{26}$$

Using the principle of analogy, one very complicated nonlinear problem may be solved as a simpler linear dynamical one. Consequently, each isochronous stress-strain diagram can be accurately approximated by the RDA.

3.2 Rheological-Dynamical and EC 2 limit Analysis

Description of the highly complex behavior of concrete is a difficult task and to date generally accepted constitutive equations do not exist. A variety of models have been proposed to characterize the stress-strain relations and failure behavior. All these models have certain inherent advantages or disadvantages which depend to a large degree on the particular application considered.

Analytical procedure, based on the model of viscoelastoplastic material and RDA, which can be used to predict the buckling strength and determine the buckling curves of columns, was introduced by Milašinović [4]. Goleš [5] noticed that the application of this procedure is limited to a certain range of slenderness, so characteristic load-bearing capacity of two-hinged concrete column may be expressed as follows

$$\sigma_{cr}(t) = \begin{cases} \dfrac{\pi^2}{(L/k_z)^2}E_H & for\ \lambda = \dfrac{L}{k_z} \geq \lambda_E \\ E_R(t)E_H = \dfrac{E_H}{\left(\dfrac{L}{k_z}\right)\dfrac{k_z^3}{I_z}\dfrac{1}{\gamma\varphi(t)}} & for\ \lambda_D \leq \lambda \leq \lambda_E\ , \\ f_{cm} & for\ \lambda \leq \lambda_D \end{cases} \tag{27}$$

where E_H is initial modulus of elasticity, $E_R(t)$ dynamic or RDA modulus, L length of the column, k_z radius of gyration, λ slenderness ratio of the column, I_z second moment of area of cross-section, γ specific gravity, $\varphi(t)$ creep coefficient, and f_{cm} mean value of concrete cylinder compressive strength. λ_E is the upper boundary, elastic slenderness value which corresponds to the intersection of Euler and RDA buckling curves, while λ_D represents the lower slenderness limit of applicability of RDA procedure. λ_D is slenderness ratio that corresponds to the intersection point of RDA improved buckling curve and horizontal line which represents the mean value of concrete cylinder compressive strength f_{cm} (Fig. 3). The critical buckling stress obtained for λ_D is equal to f_{cm}, and stress-strain diagram, which is provided by the RDA procedure for slenderness ratio λ_D, is also valid for all less slenderness ratios.

Because of this, the working diagrams for concrete of various strength classes can be obtained by applying the RDA procedure on the standard specimen (cylinder) for testing compressive strength of concrete, if the mean value of concrete cylinder compressive strength f_{cm}, secant modulus of elasticity of concrete E_{cm}, specific gravity γ and Poisson's ratio μ. are known. If μ is unknown, it may be determined from the criterion that the compressive strain at the peak stress f_{cm} takes the value given in EC 2.

The procedure consists of several steps. First, RDA buckling curve is drown according to Eq. (28)

$$\sigma_{RDA} = \frac{E_{cm}}{\lambda \frac{k_z^3}{I_z} \frac{1}{\gamma \varphi^*}}, \tag{28}$$

where φ^* is the structural creep coefficient, which represents the creep coefficient at the limit of elasticity and, according to Ref. [6], may be expressed as follows

$$\varphi^* = \left[\left(\frac{1}{1-\mu\varepsilon_E} \right)^4 - 1 \right] \cdot \frac{1}{2\varepsilon_E} \Bigg/ \left\{ 1 - \left[\left(\frac{1}{1-\mu\varepsilon_E} \right)^4 - 1 \right] \cdot \frac{1}{2\varepsilon_E} \right\}. \tag{29}$$

ε_E is the strain at the limit of elasticity. It is observed [5] that the value of φ^* depends very little on ε_E, so, for concrete, the value of ε_E=0.0003 can be adopted.

Slenderness ratio λ_E is obtained from the terms of intersection of Euler and RDA buckling curves

$$\lambda_E = \pi^2 \frac{k_z^3}{I_z} \frac{1}{\gamma \varphi^*}. \tag{30}$$

Stress and strain at the limit of elasticity are as follows

$$\sigma_E = \frac{\pi^2}{\lambda_E^2} E_{cm}, \quad \varepsilon_E = \frac{\sigma_E}{E_{cm}}. \tag{31}$$

When stresses exceed the elasticity border, the modulus E_{cm} is not constant any more. It becomes equal to the dynamic RDA modulus $E_R(t)$. As $\sigma(t)$ increases $E_R(t)$ decreases. Thus, the use of relation $E_R(t)$ v/s $\sigma(t)$ may improve the results of Eq. (28). Let us assume sinusoidal stress excitation

$$\sigma(t) = \sigma_{RDA} \sin(\omega_\sigma t). \tag{32}$$

The corresponding creep coefficient is as follows

$$\varphi(t) = \sigma(t) \frac{l_E}{k_z} \frac{k_z^3}{I_z} \frac{1}{E_H} \frac{1}{\gamma} = \sigma(t) K_\varphi, \tag{33}$$

where K_φ is the constant for the column

$$K_\varphi = \frac{l_E}{k_z} \frac{k_z^3}{I_z} \frac{1}{E_H} \frac{1}{\gamma}. \tag{34}$$

Now dynamic RDA modulus [4] becomes

$$E_R(t) = \frac{\frac{1+\delta^2}{E_H(t_0)} + \frac{1}{E_K^D(t)}}{\frac{1+\delta^2}{E_H^2(t_0)} + \frac{1}{E_K^D(t)} \left(\frac{2}{E_H(t_0)} + \frac{1}{E_K^D(t)} \right)}, \tag{35}$$

where

$$\omega_\sigma = \frac{\pi}{2t_E}, \quad \delta = \frac{\pi}{2t_E} T_K^D \text{ and } E_K^D = \frac{E_H}{\varphi(t)}. \tag{36}$$

The time t_E when stress reaches the point of elasticity is experimentally determined value. The function $E_R(t)$ v/s $\sigma(t)$ may be found explicitly. Now, for the computed value of σ_{RDA}, according to Eq. (28), appropriate E_R may be selected and then recalculated a new σ_{RDA}. This iterative procedure must be performed until there is convergence to the stress σ_{RDAI}, which represents the compressive strength of observed column of slenderness ratio λ. The procedure repeats for different slenderness ratios, and improved RDA buckling curve can be drowned. The lower slenderness limit λ_D for the reference sample (cylinder) can be found from the intersection of this curve and the horizontal line corresponding to the mean value of concrete compressive strength - Fig. 3. RDA working diagram determined for lower slenderness limit λ_D is also valid for all smaller slenderness ratios, including the actual slenderness ratio of the sample (λ=8).

The stress-strain diagram of uniaxial compressed concrete column of slenderness ratio λ_D can be obtained by an iterative RDA procedure, starting from the known strain at the elastic limit ε_{el} Eq. (31). For *i-th* step is obtained

$$E_{Ri} = \frac{\sigma_i - \sigma_{i-1}}{\varepsilon_i - \varepsilon_{i-1}} \Rightarrow \varepsilon_i = \frac{\sigma_i - \sigma_{i-1}}{E_{Ri}} + \varepsilon_{i-1}, \tag{37}$$

and follows

$$\varepsilon_{el} = \frac{\sigma_E}{E_H}, \quad \varepsilon_1 = \frac{\sigma_1 - \sigma_E}{E_{R1}} + \varepsilon_{el}, \quad \varepsilon_2 = \frac{\sigma_2 - \sigma_1}{E_{R2}} + \varepsilon_1,$$

$$\varepsilon_i = \frac{\sigma_i - \sigma_{i-1}}{E_{Ri}} + \varepsilon_{i-1}, \quad \varepsilon_{RDAI} = \frac{\sigma_{RDAI} - \sigma_n}{E_{RDAI}} + \varepsilon_n,$$

$$\varepsilon_{vp} = \frac{\sigma_{RDA} - \sigma_{RDAI}}{E_H} + \varepsilon_{RDAI}. \tag{38}$$

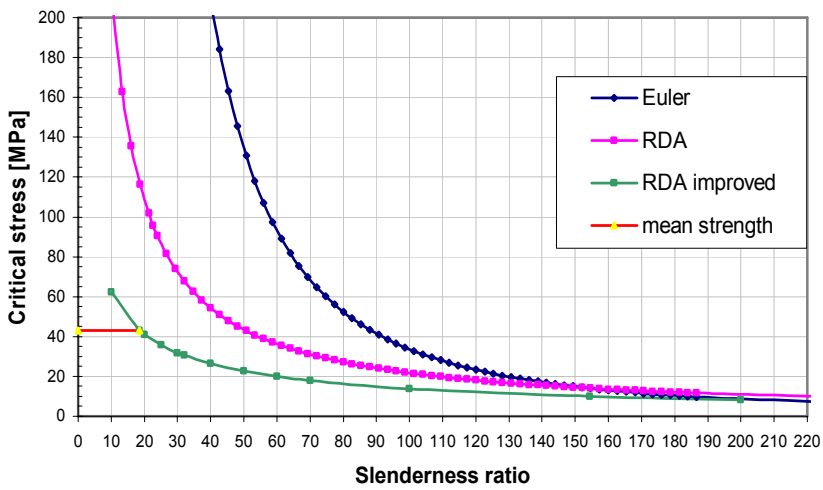

Figure 3: Buckling curves and mean value of concrete cylinder compressive strength for concrete of grade C35/45

Fig. 4 gives comparison of working diagram of concrete C35/45 according to Eurocode 2 and RDA, under the short-term uniaxial pressure. For comparison is adopted stress-strain diagram given by EC 2 for the nonlinear analysis of structures, according to the expression

$$\frac{\sigma_C}{f_{cm}} = \frac{k\eta - \eta^2}{1+(k-2)\eta}, \tag{39}$$

where $\eta=\varepsilon_c/\varepsilon_{c1}$, ε_{c1} is the strain at the peak stress (ε_{c1}=2.25‰) and

$$k = 1.1E_{cm} \cdot |\varepsilon_{c1}| / f_{cm}. \tag{40}$$

According to RDA the maximum strain is ε_{cu1}=4.447‰. For practical application, it is recommended to limit the value of this strain to ε_{cu1}=3.5‰, as in EC 2.

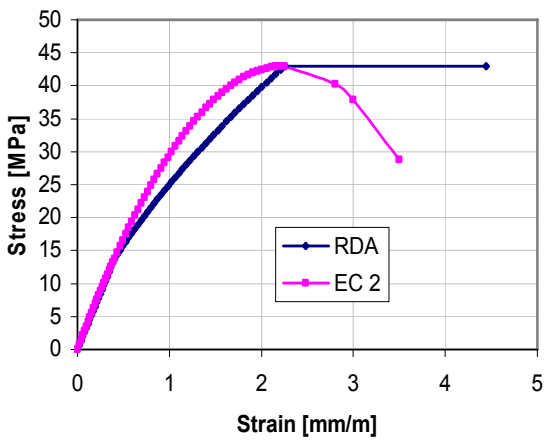

Figure 4: Comparison of working diagrams of concrete C35/45 according to EC 2 and RDA

Milašinović [6] gave a detailed description of the iterative RDA procedure for obtaining the stress-strain diagram of a steel rod, when its coefficient of linear thermal expansion α_T, specific heat c, mass density ρ, modulus of elasticity E_H and slenderness ratio at the point of elasticity λ_E are known. He experimentally verified the procedure on the prototype. On the basis of known physical parameters of material, established by the prototype, and basic mechanical parameters of steel bars, that are standard tested, Goleš in [5] theoreticaly obtained RDA stress-strain diagrams of reinforcement. Modulus of elasticity E_H and yield stress σ_Y of reinforcement are adopted according to declaired properties of material ($\sigma_Y=f_{yk}$, $E_H=E_S$). Structural creep coefficient can be calculated from Eq. (29), whith adopted ε_E=0.001 and Poisson's ratio μ=1/3. Elasticity stress and corresponding strain can be determined from [6]

$$\sigma_E = \sigma_Y \frac{\varphi^*}{1+\varphi^*}, \quad \varepsilon_E = \frac{\sigma_E}{E_H}. \tag{41}$$

Slenderness ratio of the fictitious sample (or true model) can be determined from the first term in (27) as folows

$$\lambda_E = \lambda_{tm} = \sqrt{\frac{E_H \pi^2}{\sigma_E}} \,. \tag{42}$$

Relation between the true model and the prototype, both of circular cross-sections, according to Ref. [5] may be written as

$$l_{0,tm} = l_{0,pr} \frac{\phi_{tm}}{\phi_{pr}} \sqrt{\frac{\varepsilon_{p,pr}}{\varepsilon_{p,tm}}} \,, \tag{43}$$

where $l_{o,tm}$ and $l_{o,pr}$ are lengths of the true model and the prototype, ϕ_{tm} and ϕ_{pr} their diameters, $\varepsilon_{p,tm}$ and $\varepsilon_{p,pr}$ their proportional strains. With $\lambda=4l_0/\phi$, proportional strain and stress of true model can be determined as follows

$$\varepsilon_{p,tm} = \varepsilon_{p,pr} \frac{\lambda_{pr}^2}{\lambda_{tm}^2} = \varepsilon_p \,, \quad \sigma_p = E_H \varepsilon_p \,. \tag{44}$$

Iterative procedure continues as in Ref. [6]. According to Ref. [5], the number of iterations in viscoelastoplastic (VEP) range depends on type of steel. For the reinforcement RA 400/500 (B400) whith mechanical characteristics: f_{yk}=400MPa, f_{tk}=500MPa, $\varepsilon_{uk}\geq$10%, E_s=200GPa, number of iterations should be between i=2 and i=5. Lower yield point, for this steel, should be neglected. The stress-strain diagram for this steel, obtained by RDA iterative procedure, is shown in Fig. 5a. The diagram in Fig. 5b is drown for the same steel, accoding to EC 2.

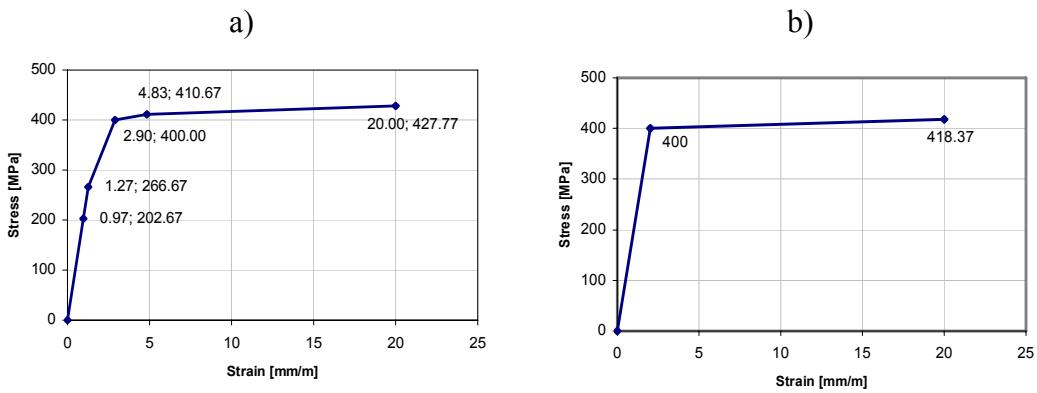

Figure 5: Working diagrams of steel B400, for the bar diameter Ø19mm, according to a) - RDA and b) - EC 2

4 Applications

An reinforced concrete 20m long simple supported folded plate structure, with applied vertical uniformly distributed load: self-weight of structure g, self-weight of covering on sloped planes Δg=0.5kN/m^2 and snow load on sloped planes s=1.0kN/m^2 (Fig. 6), is analyzed. The structure is made of concrete C35/45 and reinforcement B400. Linear FSM analysis for 10 strips and 100 series terms is performed using elasticity modulus of E=34GPa and Poisson's ratio μ=0. Diagrams of internal forces and bending moments along the transverse central cross-section are shown in Fig. 7.

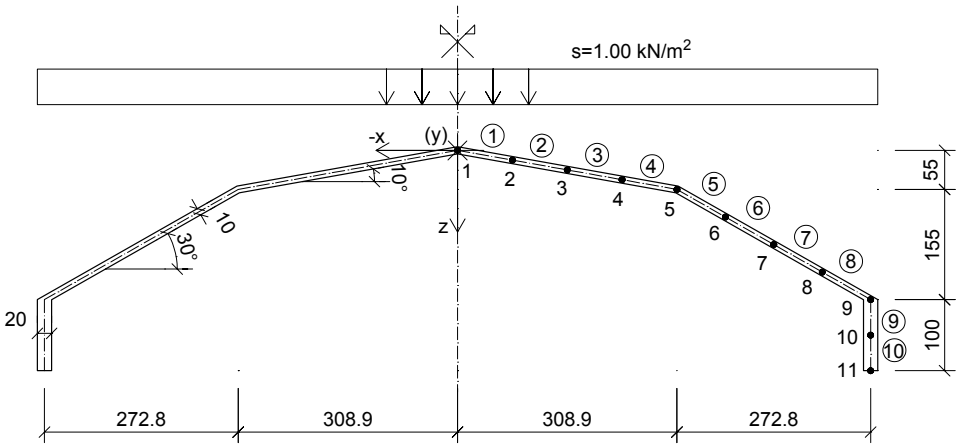

Figure 6: Cross-section of analysed folded plate structure

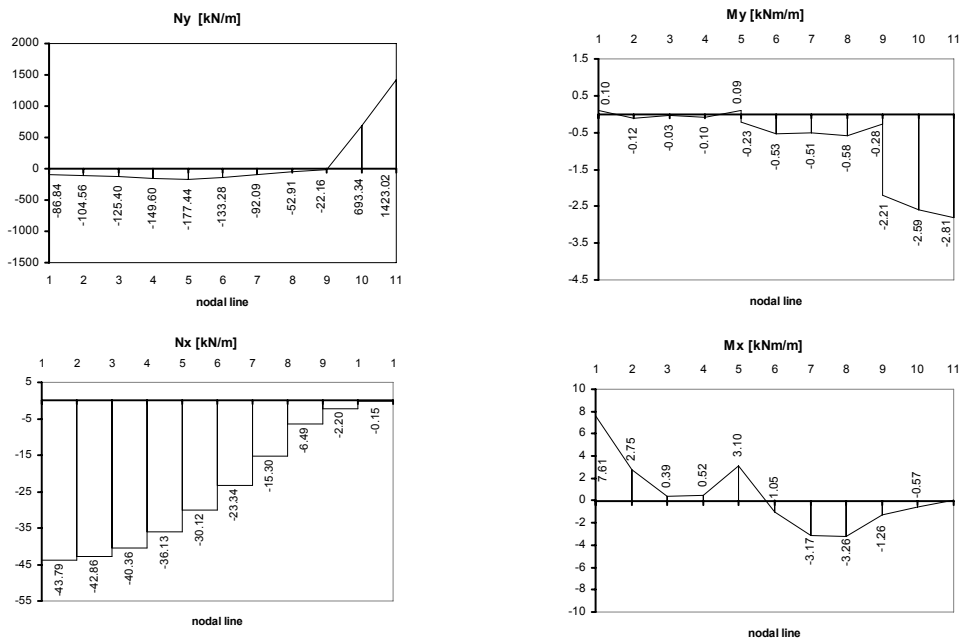

Figure 7: Internal forces and bending moments along the transverse central cross-section, according to linear elastic FSM

Limit state design (ultimate and serviceability) of characteristic cross sections is performed according to currently valid Serbian technical regulations for concrete and reinforced concrete, using partial factor method. Diagrams of interaction (N_u-M_u) of two characteristic cross sections are drawn using various combinations of working diagrams (WD) of concrete and steel according to Eurocode 2 and according to RDA (A-both WD according to EC 2; B-both WD according to RDA, without strain limitation in concrete; C-both WD according to RDA, with limited maximum strain in concrete to ε_{cu}=3.5‰; D-RDA WD of steel and EC 2 WD of

concrete; E-EC 2 WD of steel and RDA WD without strain limitation of concrete and F-EC 2 WD of steel and RDA WD with limited maximum strain in concrete to ε_{cu}=3.5‰) – Figs. 8 and 9. Partial safety factors for material are not applied. Tension force is treated as negative. Positive bending moment of the border beam stretches the bottom side of cross-section.

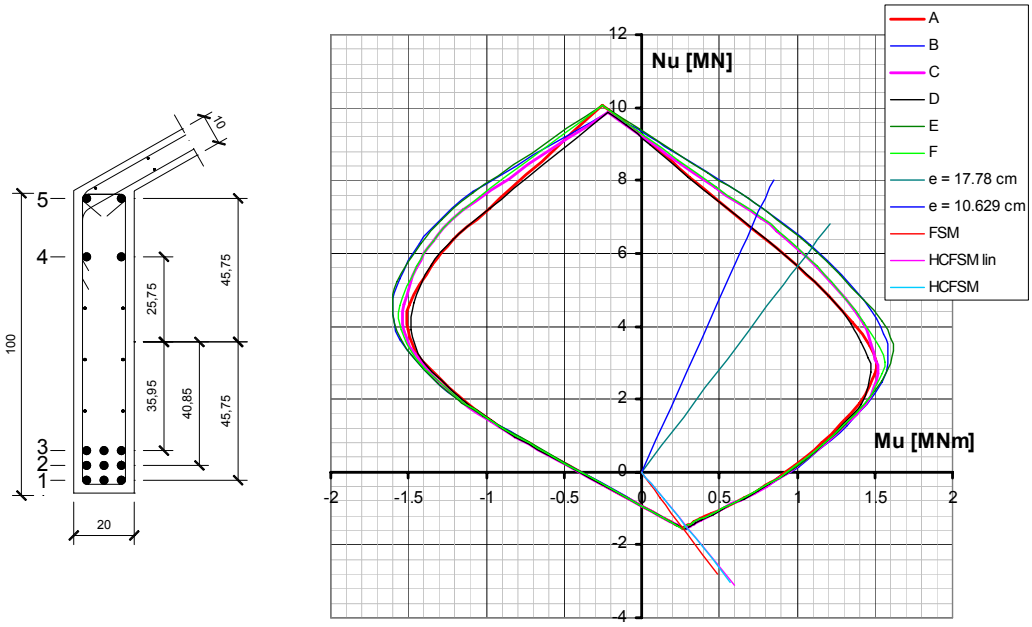

Figure 8: Cross-section of the border beam with reinforcement Ø19mm and corresponding N_u-M_u diagram

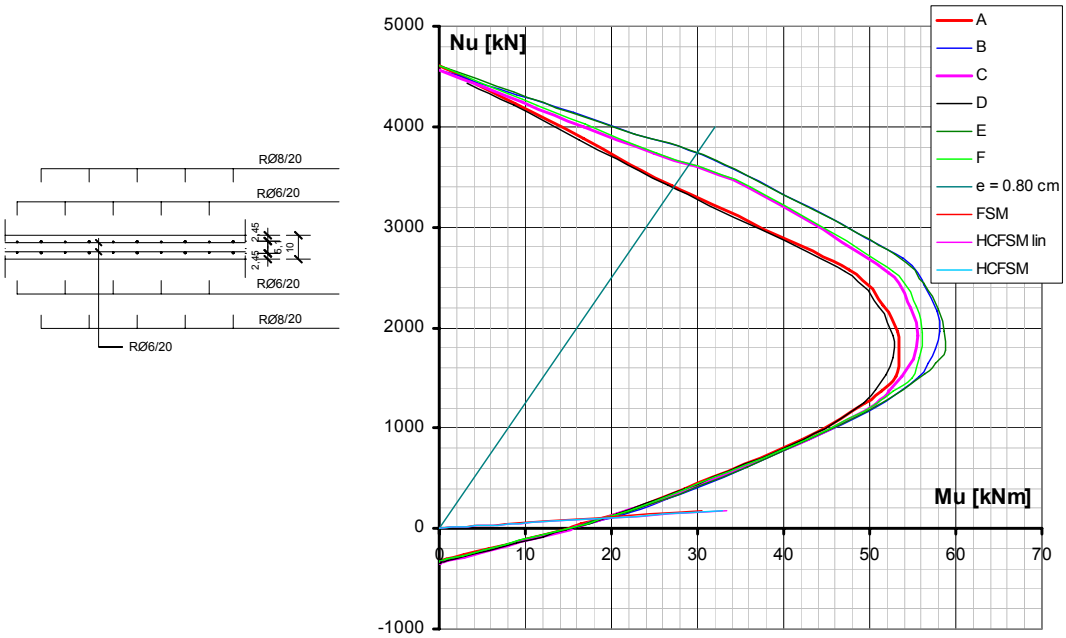

Figure 9: Cross-section in nodal line 1 and corresponding N_u-M_u diagram

The ultimate resistance (N_u) and global safety factors $\gamma=N_u/N$ of two selected cross-sections are shown in Table 1. Eccentricity of normal force due to applied actions is $e=M/N$, where M and N are bending moment and normal force calculated by FSM, linear HCFSM and nonlinear HCFSM. In the case of nonlinear HCFSM, only the Green-Lagrange predictions are compared, because the von Karman solutions are almost similar to those from linear HCFSM. It has to be noted that applied load in HCFSM slightly differ from that shown in Fig. 4 (variable uniformly distributed load is added at the border beam). That is the reason why the effects of applied loads for linear HCFSM differ from those of FSM.

		Combination of working diagrams of concrete and steel					
		A	B	C	D	E	F
border beam							
FSM	effects of applied load	N=-696.75kN; M=121.05kNm; e=-0.17373m					
	N_u	-1530	-1570	-1570	-1570	-1530	-1530
	γ	2.20	2.25	2.25	2.25	2.20	2.20
linear HCFSM	effects of applied load	N=-779.66kN; M=149.60kNm; e=-0.19188m					
	N_u	-1490	-1520	-1520	-1520	-1490	-1490
	γ	1.91	1.95	1.95	1.95	1.91	1.91
nonlinear HCFSM	effects of applied load	N=-765.27kN; M=143.91kNm; e=-0.18805m					
	N_u	-1505	-1535	-1535	-1535	-1505	-1505
	γ	1.97	2.01	2.01	2.01	1.97	1.97
cross-section in nodal line 1							
FSM	effects of applied load	N=43.79kN; M=7.61kNm; e=0.17379m					
	N_u	107.60	116.52	113.64	112.78	112.49	110.48
	γ	2.46	2.66	2.60	2.58	2.57	2.52
linear HCFSM	effects of applied load	N=44.57kN; M=8.35kNm; e=0.18735m					
	N_u	98.75	105.15	104.08	102.75	102.21	101.68
	γ	2.22	2.36	2.34	2.31	2.29	2.28
nonlinear HCFSM	effects of applied load	N=44.22kN; M=8.22kNm; e=0.18589m					
	N_u	99.52	107.59	105.98	103.56	103.29	103.02
	γ	2.25	2.43	2.40	2.34	2.33	2.33

Table 1 - The ultimate resistance and global safety factors of two cross sections

Nonlinear geometric effects which are of major importance in the deformational response as well ultimate and serviceability load analysis of longer reinforced concrete folded shells are used in order to examine structure stability.

The comparative efficiency of the von Karman and the Green-Lagrange HCFSM solutions is presented in the large-displacement stability analysis. Various span lengths (10, 15, 20, 25 and 30m) of structure and various series terms (1, 3, 5-29 and 31) are considered in the analysis. The convergence is established when the norm of the residual forces value is less or equal to 0.1 (accuracy 1/1000). The total loading was divided into 8 (0.6, 0.04, 0.04, 0.04, 0.04, 0.04, 0.1 and 0.1) increments of load. The load factor 0.8 corresponds to the service load.

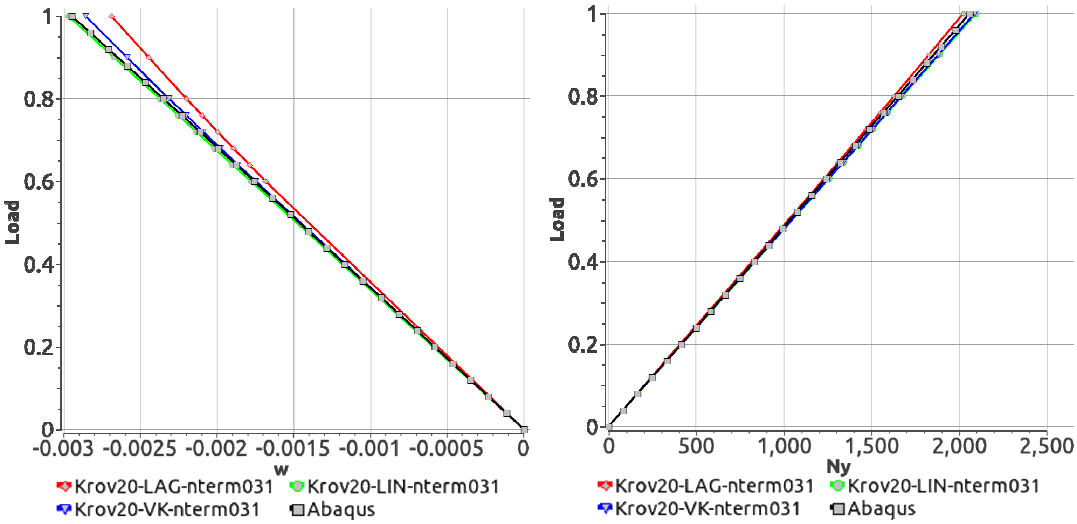

Figure 10: Variation of central deflection w in nodal line 1 and normal force N_y in nodal line 11 with load intensity

As shown in Fig. 10, the effect on nonlinear behavior is less pronounced in the 20m long structure. In this example the response always involves a hardening structure.

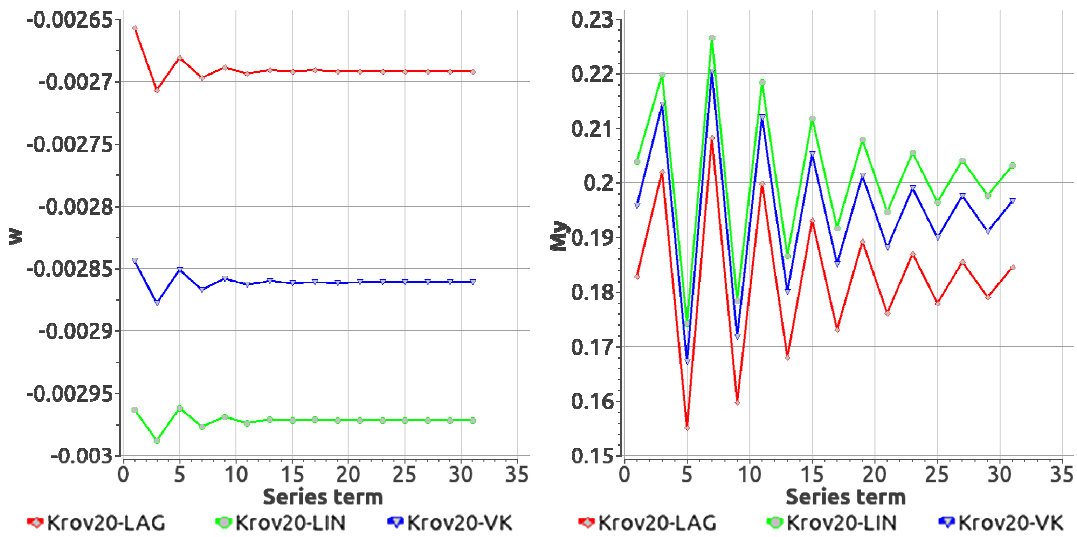

Figure 11: HCFSM convergence of central deflection w and moment M_y at the nodal line 1 for the last loading level

Fig. 11 illustrates the convergence of the deflection w and the moment M_y. The convergence is non-monotonic for all predictions: Green-Lagrange (LAG), von Karman (VK), and linear (LIN). However, the convergence of the moment M_y is poor, and many more series terms would be required for the moment values to converge to the exact answer.

The corresponding increment of load in term of TSMS eigenvalue is depicted in Fig. 12. To illustrate the static equilibrium in the context of stability, the load-part curves which corresponds to stable equilibrium states is plotted with solid line, while the load-part curves which corresponds to unstable equilibrium states is plotted with a dashed line. Analysis of the influence of the load on TSMS eigenvalue was demonstrated to all span lengths (10, 15, 20, 25 and 30m) and 31 series terms adopted in the computations. For all structures the stability regions were observed for both the von Karman and the Gree-Lagrange predictions under all load increment. It was stated that span length have a serious influence on equilibrium state. Consequently when span length increases a drop of TSMS eigenvalue is observed. Also that when load increases the rise of TSMS eigenvalue was observed for both the von Karman and the Green-Lagrange predictions. It is in accordance with the response which involves a hardening structure for 20m span length.

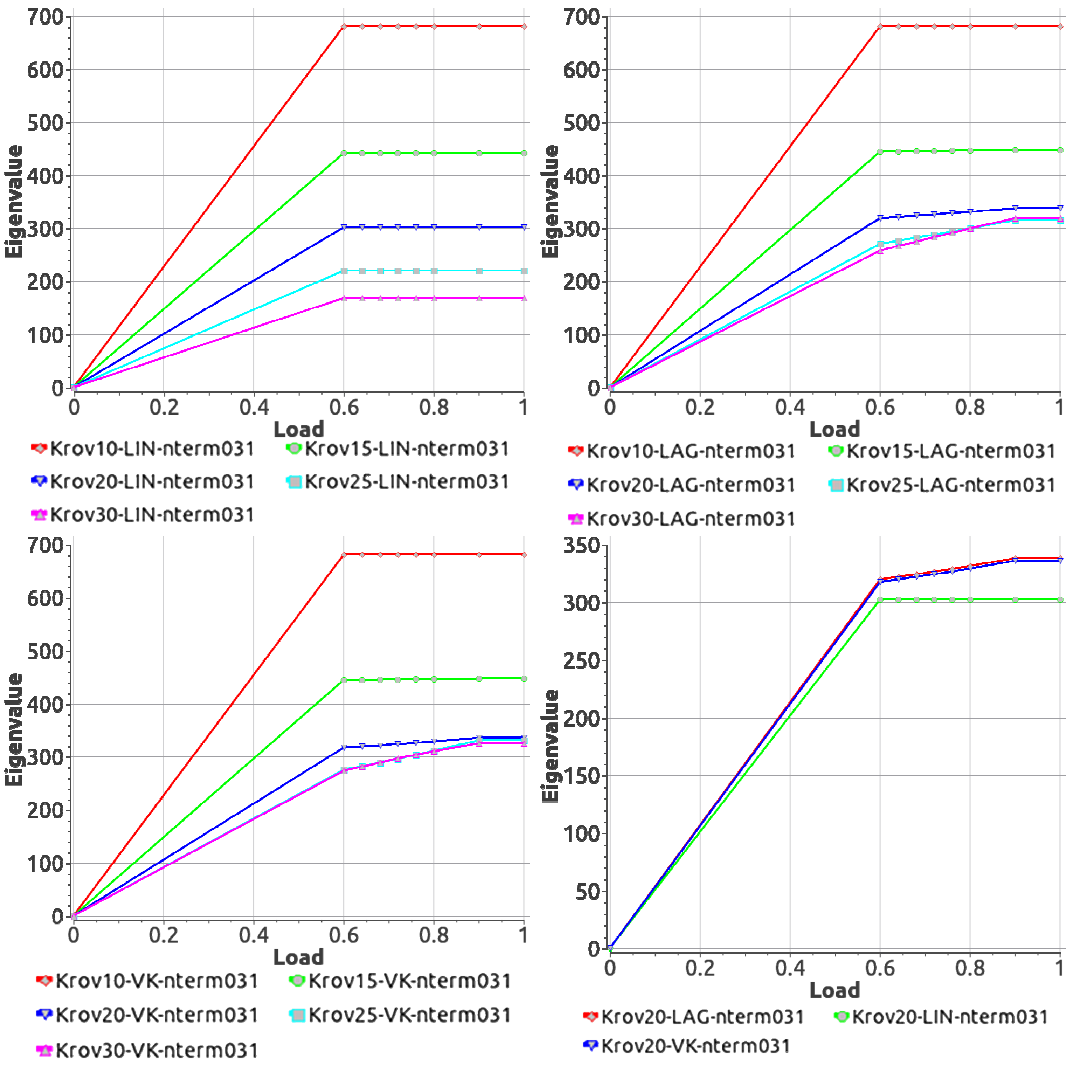

Figure 12: Variation of TSMS eigenvalue with load intensity for inputs with different structure span lengths and 31 series terms involved in computations

5 Comparative Finite Element Analysis

During the research, we compared HCFSM results with those obtained in ABAQUS with shell elements. The variations of central deflection w in nodal line 1 and normal force N_y in nodal line 11 with load intensity are presented in Fig. 10. We used STRI3 element which is the only element in ABAQUS library that is intended to use for thin plates imposing the Kirchof's theory [7]. This element models arbitrarily large rotations but only small strains.

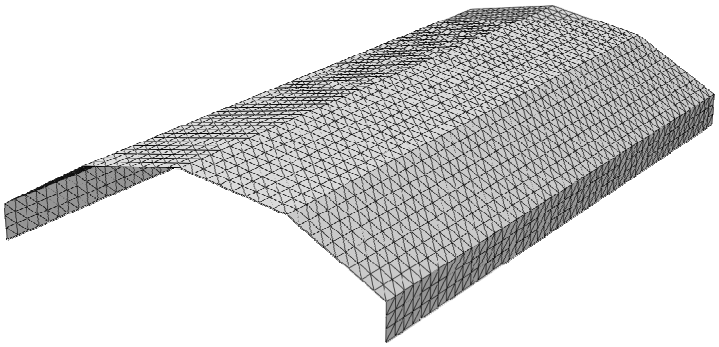

Figure 13: Shell model in ABAQUS with 3800 STRI3 elements

The uniform mesh size shown in Fig. 13 has been varied for convergence study. Fig. 14 presents central deflection convergence.

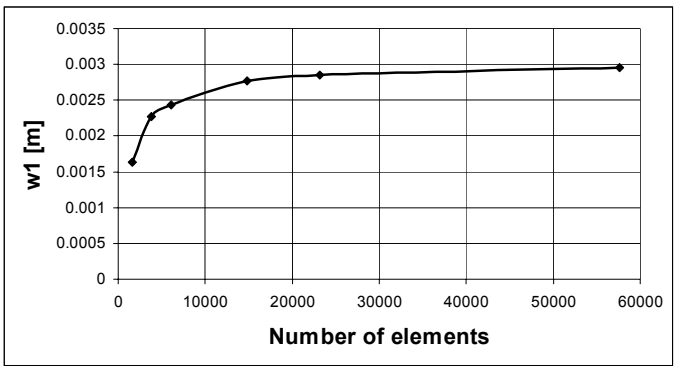

Figure 14: ABAQUS convergence of central deflection

6 Conclusions

The HCFSM computational model for the analysis of reinforced concrete folded plates has been described and the results of several numerical applications with comparative finite element analysis has been presented and discussed. Good correlation was found between the HCFSM and the FEM results throughout the entire structural response for 20m span length, which demonstrates the effectiveness

of the HSFSM code. Geometric nonlinear effects need to be taken into consideration in order to obtain realistic numerical solutions for longer shells because that span length has a serious influence on equilibrium state. When the lowest eigenvalue of the tangential stiffness matrix of structure becomes negative, a bifurcation state can be missed when using a finite element program if this matrix is not calculated and checked. A variation in the RDA stress-strain diagrams of concrete and reinforcement has a negligible influence on the ultimate load compared with EC 2 for shorter shells, as long as a collapse mechanism based on the EC 2 for nonlinear analysis is developed. However, as the cracked concrete model depends on the existing strain field, a rigorous convergence criterion in terms of displacements and dynamic RDA modulus should be adopted.

Acknowledgements

The work reported in this paper is a part of the investigation within the research projects: ON174027 "Computational Mechanics in Structural Engineering" and TR 36017 "Utilization of by-products and recycled waste materials in concrete composites in the scope of sustainable construction development in Serbia: investigation and environmental assessment of possible applications", supported by the Ministry for Science and Technology, Republic of Serbia. This support is gratefully acknowledged.

References

[1] Y.K. Cheung, Finite Strip Method. CRC Press LLC, 1998.

[2] D.D. Milašinović, The Finite Strip Method in Computational Mechanics. Faculties of Civil Engineering: University of Novi Sad, Technical University of Budapest and University of Belgrade: Subotica, Budapest, Belgrade, 1997.

[3] Z.P. Bažant, L. Cedolin, Stability of Structures: Elastic, Inelastic, Fracture, and Damage Theories. Oxford University Press, Oxford, 1991.

[4] D.D. Milašinović, Rheological-dynamical analogy: prediction of buckling curves of columns. International Journal of Solids and Structures 37, 3965-4004, 2000.

[5] D. Goleš, Rheological-dynamical analysis of reinforced concrete folded plates. Doctoral thesis, University of Novi Sad, Faculty of Civil Engineering Subotica, 2012.

[6] D.D. Milašinović, Rheological-dynamical analogy: visco-elasto-plastic behaviour of metallic bars. International Journal of Solids and Structures 41, 4599-4634, 2004.

[7] Abaqus, Theory manual, version 6.7, Dassault systems, 2007.